High-Performance Integrated Self-Package Flexible Li–O_2 Battery Based on Stable Composite Anode and Flexible Gas Diffusion Layer

Xiao-yang Yang, Ji-jing Xu, Di Bao, Zhi-wen Chang, Da-peng Liu, Yu Zhang, and Xin-Bo Zhang*

With the rising development of flexible and wearable electronics, corresponding flexible energy storage devices with high energy density are required to provide a sustainable energy supply. Theoretically, rechargeable flexible Li–O_2 batteries can provide high specific energy density; however, there are only a few reports on the construction of flexible Li–O_2 batteries. Conventional flexible Li–O_2 batteries possess a loose battery structure, which prevents flexibility and stability. The low mechanical strength of the gas diffusion layer and anode also lead to a flexible Li–O_2 battery with poor mechanical properties. All these attributes limit their practical applications. Herein, the authors develop an integrated flexible Li–O_2 battery based on a high-fatigue-resistance anode and a novel flexible stretchable gas diffusion layer. Owing to the synergistic effect of the stable electrocatalytic activity and hierarchical 3D interconnected network structure of the free-standing cathode, the obtained flexible Li–O_2 batteries exhibit superior electrochemical performance, including a high specific capacity, an excellent rate capability, and exceptional cycle stability. Furthermore, benefitting from the above advantages, the as-fabricated flexible batteries can realize excellent mechanical and electrochemical stability. Even after a thousand cycles of the bending process, the flexible Li–O_2 battery can still possess a stable open-circuit voltage, a high specific capacity, and a durable cycle performance.

To open the door to the next-generation electronic environment, well-matched and high-performance flexible power sources will be key, with special advantages, such as being bendable, wearable, lightweight, foldable, and having potentially implantable properties.[1–6] However, current conventional power sources are too bulky and rigid to be integrated into flexible devices.[7] Although several inspirational prototypes have been developed, including flexible lithium-ion batteries,[8–13] supercapacitors,[14–21] and solar cells,[22–26] the low theoretical energy density of these systems still intrinsically limits their application in next-generation flexible devices.[27–29] Rechargeable lithium–oxygen (Li–O_2) batteries can deliver exceptionally high theoretical energy density[30–36] of 3600 Wh kg^{-1} (based on the reversible reaction of $2Li + O_2 \rightarrow Li_2O_2$), which holds great promise for their use in next-generation flexible electronics. However, thus far, there are only very few reports on the construction of flexible Li–O_2 batteries, and numerous technological and structural challenges must be overcome.[37–39]

Conventional flexible Li–O_2 batteries are simple assemblies of a gas diffusion layer, a cathode, a separator, and an anode that is then packed with aluminum soft packaging or shrinkable tubing.[39,40] This assembly leads to a loose battery structure, preventing bending ability and mechanical stability. During the repeated bending process, uneven force will occur along the battery and cause local stress concentration, which will inevitably influence the battery structure, cause electrode wrinkle deformation, and breakdown. Serious safety problems might occur or even failure of the battery. Moreover, the poor resilience and low plasticity of conventional flexible Li–O_2 batteries make it difficult for them to be integrated into flexible devices. A conventional gas diffusion layer nickel foam and anode Li foil, both of which have poor mechanical properties that seriously restrict their application in flexible Li–O_2 batteries. All these limitations severely restrict the application of Li–O_2 batteries as flexible energy storage devices. Therefore, it is necessary to design and fabricate an integrated flexible Li–O_2 battery with super structure stability based on a new type of gas diffusion layer and an anode with high mechanical stability.

Herein, we developed an integrated flexible Li–O_2 battery (IFLB) based on a high-fatigue-resistance anode and a novel flexible stretchable gas diffusion layer. Owing to the excellent mechanical properties and flexible ability of the new type of composite anode and gas diffusion layer, the obtained IFLB can fully recover even after being bent into various shapes thousands of times, demonstrating superior mechanical and

X.-y. Yang, Dr. D.-p. Liu, Prof. Y. Zhang
Key Laboratory of Bio-Inspired Smart Interfacial Science and Technology of Ministry of Education
School of Chemistry and Environment
Beihang University
Beijing 100191, P. R. China
E-mail: jade@buaa.edu.cn

X.-y. Yang, Dr. J.-j. Xu, Dr. D. Bao, Z.-w. Chang, Prof. X.-B. Zhang
State Key Laboratory of Rare Earth Resource Utilization
Changchun Institute of Applied Chemistry
Chinese Academy of Sciences
Changchun 130022, P. R. China

DOI: 10.1002/adma.201700378

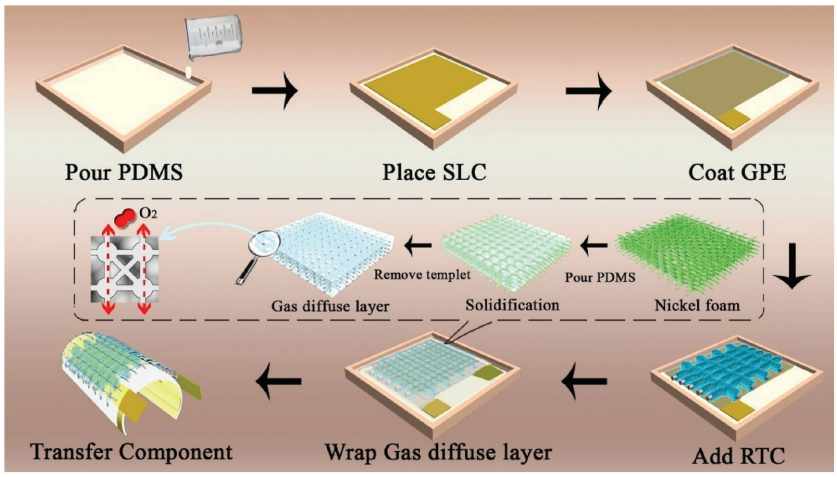

Figure 1. Schematic illustration of the fabrication of the integrated, flexible Li–O_2 battery (inset diagram illustrates the process of making the gas diffusion composite layer).

flexibility stability. Polydimethylsiloxane (PDMS) is widely used in the flexible device field; thus, the IFLB can be conveniently integrated with other commercial flexible products to form an all-in-one flexible system. Significantly, with the synergistic effect of the high electrochemical activities of the combination of RuO_2 and TiO_2 and the tailored hierarchical structure of the electrode, the IFLB delivers superior electrochemical performance, including a high specific capacity, good rate capability, and cycling stability.

Figure 1 is a schematic representation of the IFLB composed of a PDMS substrate, a stainless steel mesh–Li–Cu (SLC) composite foil anode, a gel polymer electrolyte (GPE), a flexible, free-standing cathode, and a flexible, stretchable gas diffusion layer. First, the liquid PDMS polymer was poured into a mold as a substrate. A piece of SLC anode was then placed in the center of the substrate, followed by coating a layer of GPE as a separator and to prevent exposure of the anode to moisture.[40] After that step, the as-prepared cathode was placed and fixed with PDMS substrate. Finally, the obtained Li–O_2 battery was wrapped with a flexible, stretchable gas diffusion layer to enhance the mechanical stability and gas diffusion efficiency. After solidification in 80 °C in a glove box for 3 h, the IFLB was obtained. It is worth noting that the size of the IFLB is easy to control using this method. Stainless steel mesh, Li foil, and Cu foil were rolled together to fabricate an SLC anode; the detailed preparation process is illustrated in Figure S1 (Supporting Information). The inset in Figure 1 shows the schematic diagram of the assembly of the flexible, stretchable gas diffusion layer. The template method was introduced to construct gas diffusion layer. First, liquid PDMS was used to fill the hole of nickel foam. After heating solidification, the nickel foam template was dissolved in hydrochloric acid in an ultrasonic bath for 1 d. The gas diffusion composite was then obtained after drying at 60 °C in vacuum for 10 h.

As illustrated in **Figure 2**a, free-standing RuO_2/TiO_2 nanowires (NWs) were grown on a carbon cloth substrate mainly via a three-step process. First, the TiO_2 seeds were deposited uniformly and densely on the carbon fibers of carbon cloth to protect the carbon cloth surface and to assist the following hydrothermal reaction. After that step, free-standing TiO_2 NWs were grown in situ on carbon fibers using the seed-directed coordination self-assembly method. RuO_2 nanoparticles were then coated on the surface of TiO_2 NWs by electrodeposition. After annealing the synthesized material at 200 °C for 20 min, we obtained the final product. The scanning electron microscopy (SEM) images shown in Figure S2a in the Supporting Information reveal that pristine-CC (PC) was woven by carbon fibers with a diameter of 10 µm and that the TiO_2 NWs were uniformly and vertically grown on the framework of carbon fibers without any need of an additional binder (Figure S2b, Supporting Information) to construct a high-performance binder-free and flexible electrode foundation. Notably, the morphology of the TiO_2 NWs does not exhibit considerable change (Figure S2c, Supporting Information), with an average diameter of ≈100 nm both before and after electrodeposition. The X-ray diffraction (XRD) pattern (Figure S3, Supporting Information) illustrates that the resulting TiO_2 from the hydrothermal reaction is in rutile crystal form. Although the 200 °C annealing temperature can ensure RuO_2 generation, its small amount compared to TiO_2 and C causes its diffraction peak not to be detected in the XRD pattern. However, the transmission electron microscopy (TEM) and X-ray photoelectron spectroscopy (XPS) results clearly reveal the existence of RuO_2 on the TiO_2 NW surface. As we can see from the TEM images of a single NW, compared with a TiO_2 NW (Figure S4, Supporting Information), the core–shell configuration of RuO_2/TiO_2 (Figure 2b) can be clearly observed after electrodeposition. The high-resolution TEM (HRTEM) image inset in Figure 2b indicates that the RuO_2 nanoparticles have a lattice spacing of 0.279 nm, corresponding to the (111) crystal planes of RuO_2,[41] and the TiO_2 NWs has a lattice spacing of 0.325 nm, corresponding to the (110) crystal planes of TiO_2.[38] To further investigate the composition and distribution of the composite, we carried out energy-dispersive X-ray (EDX) mapping and Raman spectroscopy. EDX maps of Ti, O, and Ru are shown in Figure 2c. Ti and O are distributed in a banded pattern, which agrees with the morphology of the TiO_2 NWs. Ru is uniformly distributed around the TiO_2 NWs. The overlap between Ru and O suggests that the coating layer is RuO_2. Figure 2d shows the Raman spectra of the PC, TC, and RTC samples. All samples exhibit a D-band at ≈1336 cm^{-1} and a G-band at ≈1597 cm^{-1}, which are characteristic bands of carbonaceous materials. Meanwhile, the band intensities in the TC and RTC samples were significantly small: they were only ≈1/4 of those observed for the PC sample. In particular, two new peaks located at 447 and 612 cm^{-1} were observed in the TC sample; these peaks correspond to the E_g and A_{1g} modes of two TiO_2 Raman active modes. For the RTC sample, another two new peaks were observed at 509 and 627 cm^{-1}, corresponding to the two Raman active modes of RuO_2: the E_g and A_{1g} modes, respectively.[41] Furthermore, the XPS results (Figure 2e) illustrate that the high-resolution pattern of the Ru 3d peak can be

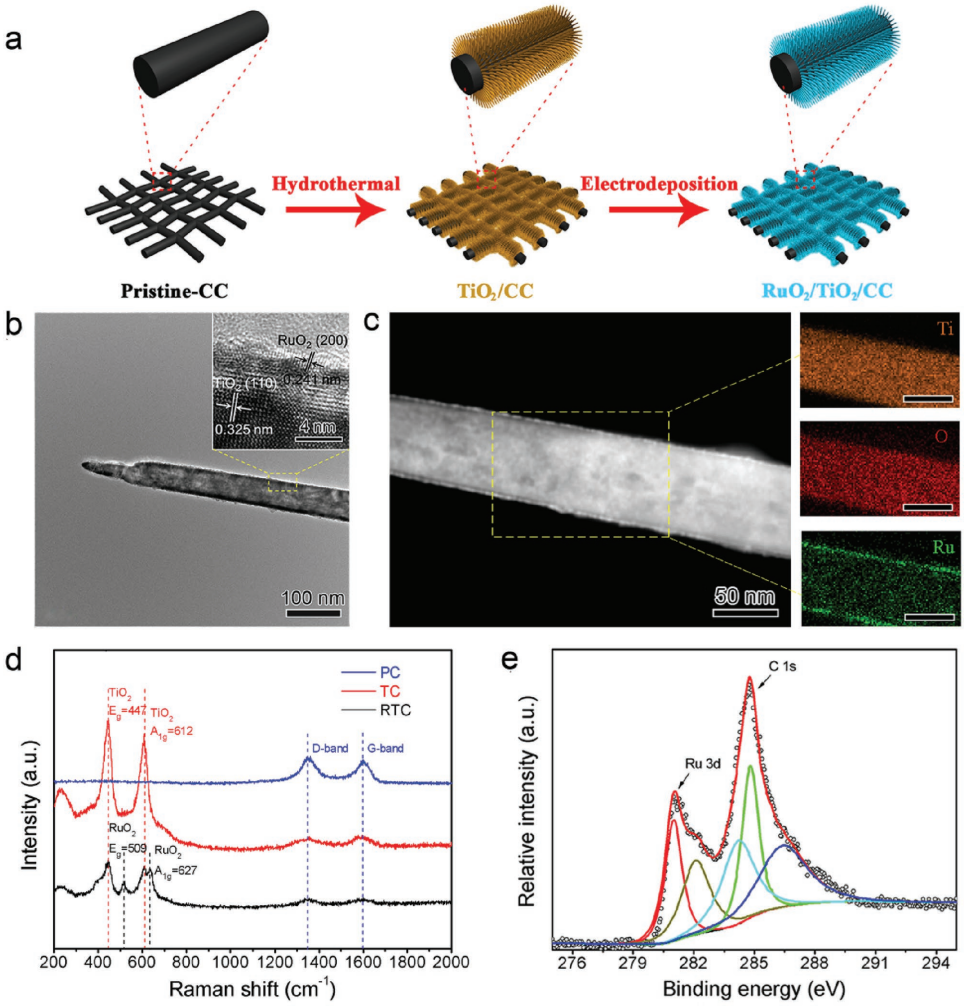

Figure 2. a) Schematic representations of the design and preparation of the RTC cathode. b) TEM image and HRTEM image (inset) of RuO_2/TiO_2 NWs. c) TEM image and the corresponding elemental mapping images (Ti, O, and Ru) of RuO_2/TiO_2 NWs. d) Raman spectra of the PC, TC, and RTC cathodes. e) C 1s and Ru 3d XPS spectra of the RTC cathode.

assigned primarily to RuO_2 (binding energy = 280.9 eV).[42,43] The pristine electrode before electrodeposition did not exhibit the RuO_2 3d peak (Figure S5, Supporting Information). These results indicate that the TiO_2 NWs were uniformly coated with RuO_2 nanoparticles at a thickness of ≈2 nm after the electrodeposition. Inductively coupled plasma mass spectrometry (ICP-MS) measurement has been carried out to ensure the atom ratio between the Ru and Ti was 1:17.3.

We constructed the IFLB to test the properties of the RTC cathode. Lithium triflate ($LiCF_3SO_3$) dissolved in tetraethylene glycol dimethyl ether was employed as the electrolyte because of its relatively high stability toward superoxide (O^{2-}). **Figure 3**a shows the comparison of the first galvanostatic discharge–charge voltage profiles and fully discharge–charge profiles (Figure S7, Supporting Information) of the flexible Li–O_2 batteries with different cathodes (PC, TC, and RTC) at a current density of 200 mA g^{-1}. In detail, the discharge–charge overpotential of the IFLB with RTC electrode is lower by ≈540 and ≈860 mV separate than those with the TC cathode and PC cathode, respectively. This result demonstrated the high catalytic activity of the RTC cathode. Cyclic voltammetry (CV) was employed to investigate the electrochemical processes of oxygen in the IFLB. The CV response of the batteries at a constant scan rate of 0.1 mV s^{-1} is presented in Figure S7 (Supporting Information). The first cycle curve reveals that the battery with the RTC cathode exhibits better oxygen reduction reaction (ORR) catalytic activity than that with the TC cathode.[44–46] Notably, at the discharge current density of 100 mA g^{-1}, the IFLB with the RTC cathode delivered a higher discharge capacity (9017 mAh g^{-1}) than that of the TC cathode (3020 mAh g^{-1}) and PC cathode (2098 mAh g^{-1}) (Figure 3b). The initial discharge curves of the Li–O_2 battery with RTC, TC, and PC cathodes under an argon (Ar) atmosphere (Figure S8, Supporting Information) were also obtained to exclude possible electrochemical contributions from the intercalation of lithium ions (Li^+) into the above cathode. It was clearly found that the background discharge capacity is negligible within the voltage range, which suggests that the oxygen reduction property of our electrode delivers excellent discharge capacity. The subsequent rate performance investigations showed that the

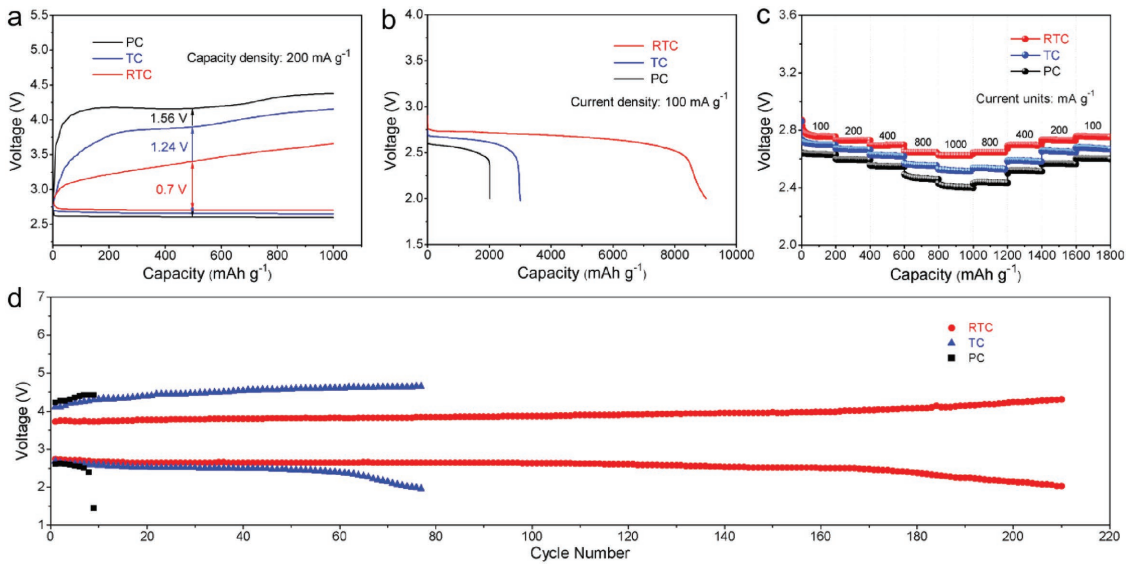

Figure 3. a) First discharge–charge curves of the Li–O_2 battery with three different cathodes at a current density of 200 mA g^{-1}. b) Full range discharge test of the Li–O_2 batteries with three different cathodes at a current density of 100 mA g^{-1}. c) The rate capability of the Li–O_2 batteries with the three types of cathodes at different current densities. d) Voltage versus cycle number on the discharge–charge terminal of the Li–O_2 cell with three different cathodes.

discharge voltage plateau of the RTC cathode is higher than that of TC and PC cathodes at each current density (Figure 3c).

Another considerable improvement of the flexible Li–O_2 battery with an RTC cathode is its cycling stability. The cycling performance of flexible Li–O_2 batteries with RTC, TC, and PC cathodes was evaluated by galvanostatic cycling at 200 mA g^{-1} with a limited capacity of 500 mAh g^{-1}. As seen in Figure 3d, the first discharge voltage of the battery with an RTC cathode is 2.73 V and stabilized at >2.0 V up to 210 cycles. By contrast, the discharge voltages of the battery with TC and PC cathodes degraded to <2.0 V after only 77 and 9 cycles, respectively. All improvements, including the specific capacities at different rates (Figure S9, Supporting Information) and the cyclic stability with the capacity limit of 1000 mAh g^{-1} (Figure S10, Supporting Information), might be attributed to the synergistic effect of RuO_2 and TiO_2 with high electrochemical activities and the tailored hierarchically free-standing structure of the electrode.

Figure 4 reveals the crystalline and morphological features of the TC and RTC cathodes after the first discharge and charge; the data demonstrate the rechargeability of the flexible Li–O_2 battery with an RTC cathode. As shown in Figure 4a, after

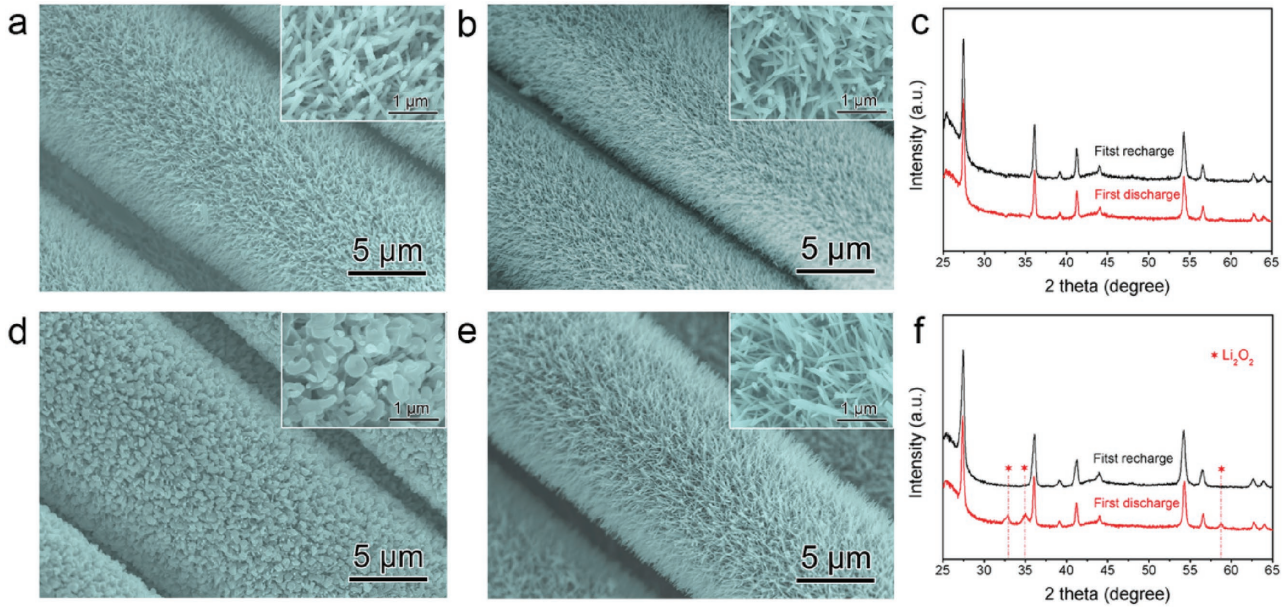

Figure 4. SEM images of the a) 1st discharge and b) 1st recharge TC cathode. SEM images of the d) 1st discharge and e) 1st recharge RTC cathode. The XRD patterns of the 1st discharge and 1st recharge c) TC and f) RTC cathode.

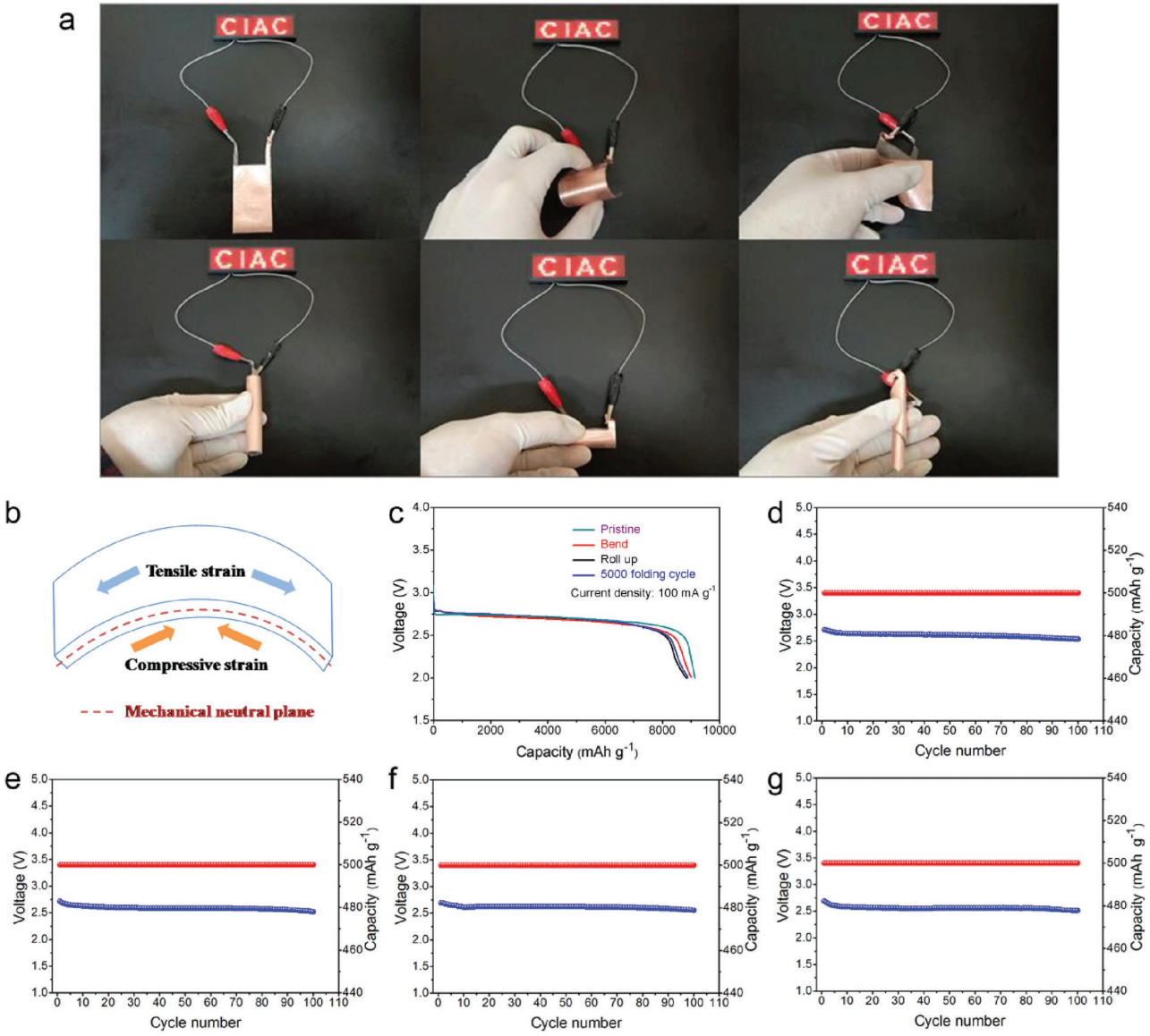

Figure 5. Integrated flexible Li–O_2 battery powering a commercial red light-emitting diode display screen at various bended and twisted conditions a). Schematic of the mechanical structure of the flexible Li–O_2 battery b). The discharge curves of the flexible Li–O_2 battery under different conditions c). The variation of terminal discharge voltage versus d–g) cycle number of the Li–O_2 batteries under various conditions.

the discharge process, a thick film of amorphous (Figure 4c) Li_2O_2 is homogenously coated onto the TiO_2 NWs of the TC cathode,[38] which will block the cathode catalytic activity and limit the further discharge process. After recharging, most discharge products can be decomposed (Figure 4b). In contrast to the above results, the well-distributed RuO_2 nanoparticles remarkably enhance the catalytic effect and increase the active sites of the electrode, and the toroidal Li_2O_2 crystal uniformly grows along the surface of the RuO_2/TiO_2 NWs like a candied gourd (Figure 4d). As a benefit of the distinctive deposited Li_2O_2 pattern and the special spatial arrangement of the RTC cathode, a highly enhanced discharge capacity can be achieved. After recharging, all discharge products disappeared, and the RTC cathode recovered to its initial state (Figure 4e). The XRD pattern (Figure 4f) and Fourier transform infrared (FTIR) spectra (Figure S11, Supporting Information) of the first discharge and recharge RTC cathode also revealed the formation and decomposition of Li_2O_2. All the above points demonstrate the high reversibility of the flexible Li–O_2 battery with the RTC cathode.

To further demonstrate the potential application of the IFLB in flexible electronics, the as-fabricated battery was used to power a light-emitting diode (LED) display screen in various bended and twisted conditions (**Figure 5**a). The stable structure and electrochemical properties under mechanical flexibility are demonstrated as follows. When the IFLB is bent with force, as shown in Figure 5b, tensile strain arises on the outer side, and compressive strain occurs on the inner side; the counterbalance between these opposite strengths incurs a space of mechanical neutrality. When the battery is settled in the mechanically neutral space by adjusting the proper thickness of PDMS capping,

compressive strain and tensile strain will not occur on the battery during the bending process, which may lead to excellent structural stability. Owing to the excellent mechanical properties of the SLC anode, the pristine structure of the anode can be maintained even after 300 bending cycles (Figure S12a,b, Supporting Information). By contrast, the structure of the pristine Li foil anode without a composite is severely damaged (Figure S12c,d, Supporting Information). Moreover, the SLC possesses higher tensile strength (54.6 MPa) than that of the pristine Li anode (5.4 MPa) (Figures S13 and S14, Supporting Information). As a benefit of the outstanding resilience of the PDMS package and the above advantages of the structure, the IFLB can easily bend into various shapes, even rolled up into an AA or AAA battery, without any damage (Figure 5a). To explore whether the deformation of the IFLB can influence the electrochemical performance, various discharge curves of the IFLB in different shapes were obtained, and the capacity did not change significantly at a current density of 100 mA g^{-1}. Surprisingly, even after 5000 folding cycles, the discharge curve of the IFLB remains almost unchanged (Figure 4c). Furthermore, the batteries remained almost constant after 100 cycles in pristine (Figure 4d), after 1000 bending cycles (Figure 4e), 1000 folding cycles (Figure 4f), and 1000 rolled up cycles (Figure 4g) conditions. The open-circuit voltage (OCV) is also recorded during repeated bending processes. As shown in Figure S15 in the Supporting Information, the OCV remains almost unchanged even after bending for 5000 cycles. All the above points demonstrate the excellent flexibility, mechanical properties, and electrochemistry stability of this newly constructed IFLB, and no structure or capability failure was observed after various flexibility tests.

In conclusion, by optimizing the battery structure, we fabricated a high-performance, flexible Li–O_2 battery with excellent mechanical stability and flexible ability based on a new type of flexible gas diffusion layer and a high-fatigue-resistance SLC anode. After introducing RTC as the cathode, superior electrochemical performance was achieved with respect to rate capability, discharge capacity, and cycling stability due to the tailored free-standing structure and superior electrochemical stability. Hence, not only are highly efficient cathodes essential for the flexible Li–O_2 battery, but each part of the flexible Li–O_2 battery, including the gas diffusion layer and anodes, must be optimized to realize high performance and long life in a flexible Li–O_2 battery with super structure stability. The results obtained here will further encourage additional studies of flexible Li–O_2 batteries, although numerous challenges restricting their application in practical devices remain.

Supporting Information

Supporting Information is available from the Wiley Online Library or from the author.

Acknowledgements

This work was financially supported by National Natural Science Foundation of China (Grant No. 51522202, 51372007, 21422108, and 51472232), and Specialized Research Fund for the Doctoral Program of Higher Education of China (20110061120040), and The Jiangsu Province Basic Research Program (grant no. BK20140267).

Keywords

composite anodes, flexible gas diffusion layers, Li–O_2 batteries, super structure stability

Received: January 19, 2017
Revised: February 4, 2017
Published online: April 24, 2017

[1] J. A. Rogers, T. Someya, Y. Huang, *Science* **2010**, *327*, 1603.
[2] A. Russo, B. Y. Ahn, J. J. Adams, E. B. Duoss, J. T. Bernhard, J. A. Lewis, *Adv. Mater.* **2011**, *23*, 3426.
[3] Y. Meng, Y. Zhao, C. Hu, H. Cheng, Y. Hu, Z. Zhang, G. Shi, L. Qu, *Adv. Mater.* **2013**, *25*, 2326.
[4] B. D. Gates, *Science* **2009**, *323*, 1566.
[5] X. Wang, X. Lu, B. Liu, D. Chen, Y. Tong, G. Shen, *Adv. Mater.* **2014**, *26*, 4763.
[6] X. Pu, L. Li, H. Song, C. Du, Z. Zhao, C. Jiang, G. Cao, W. Hu, Z. Wang, *Adv. Mater.* **2015**, *27*, 2472.
[7] L. Li, Z. Wu, S. Yuan, X.-B. Zhang, *Energy Environ. Sci.* **2014**, *7*, 2101.
[8] Q. Cheng, Z. Song, T. Ma, B. B. Smith, R. Tang, H. Yu, H. Jiang, C. K. Chan, *Nano Lett.* **2013**, *13*, 4969.
[9] S. Xu, Y. Zhang, J. Cho, J. Lee, X. Huang, L. Jia, J. A. Fan, Y. Su, J. Su, H. Zhang, H. Cheng, B. Lu, C. Yu, C. Chuang, T.-i. Kim, T. Song, K. Shigeta, S. Kang, C. Dagdeviren, I. Petrov, P. V. Braun, Y. Huang, U. Paik, J. A. Rogers, *Nat. Commun.* **2013**, *4*, 1543.
[10] H. Lin, W. Weng, J. Ren, L. Qiu, Z. Zhang, P. Chen, X. Chen, J. Deng, Y. Wang, H. Peng, *Adv. Mater.* **2014**, *26*, 1217.
[11] J. F. Ihlefeld, P. G. Clem, B. L. Doyle, P. G. Kotula, K. R. Fenton, C. A. Apblett, *Adv. Mater.* **2011**, *23*, 5663.
[12] Y. Zhang, Y. Zhao, J. Ren, W. Weng, H. Peng, *Adv. Mater.* **2016**, *28*, 4524.
[13] Y. Zhao, Z. Feng, Z. J. Xu, *Nanoscale* **2015**, *7*, 9520
[14] N. Hu, L. Zhang, C. Yang, J. Zhao, Z. Yang, H. Wei, H. Liao, Z. Feng, A. Fisher, Y. Zhang, Z. J. Xu, *Sci. Rep.* **2016**, *6*, 19777.
[15] L. Zhang, C. Yang, N. Hu, Z. Yang, H. Wei, C. Chen, L. Wei, Z. J. Xu, Y. Zhang, *Nano Energy* **2016**, *26*, 668.
[16] G. Sun, X. Zhang, R. Lin, J. Yang, H. Zhang, P. Chen, *Angew. Chem., Int. Ed.* **2015**, *127*, 4734.
[17] H. Sun, S. Xie, Y. Li, Y. Jiang, X. Sun, B. Wang, H. Peng, *Adv. Mater.* **2016**, *28*, 8431.
[18] T. Chen, R. Hao, H. Peng, L. Dai, *Angew. Chem., Int. Ed.* **2015**, *54*, 618.
[19] X. Lu, M. Yu, G. Wang, T. Zhai, S. Xie, Y. Ling, Y. Tong, Y. Li, *Adv. Mater.* **2013**, *25*, 267.
[20] W. Gao, N. Singh, L. Song, Z. Liu, A. L. M. Reddy, L. Ci, R. Vajtai, Q. Zhang, B. Wei, P. M. Ajayan, *Nat. Nanotechnol.* **2011**, *6*, 496.
[21] Z.-S. Wu, A. Winter, L. Chen, Y. Sun, A. Turchanin, X. Feng, K. Müllen, *Adv. Mater.* **2012**, *24*, 5130.
[22] Z. Liu, J. Li, F. Yan, *Adv. Mater.* **2013**, *25*, 4296.
[23] D. Liu, T. L. Kelly, *Nat. Photonics* **2014**, *8*, 133.
[24] C. Roldán-Carmona, O. Malinkiewicz, A. Soriano, G. M. Espallargas, A. Garcia, P. Reinecke, T. Kroyer, M. I. Dar, M. K. Nazeeruddin, H. J. Bolink, *Energy Environ. Sci.* **2014**, *7*, 994.
[25] J. You, Z. Hong, Y. M. Yang, Q. Chen, M. Cai, T.-B. Song, C.-C. Chen, S. Lu, Y. Liu, H. Zhou, Y. Yang, *ACS Nano* **2014**, *8*, 1674.
[26] D. Kuang, J. Brillet, P. Chen, M. Takata, S Uchida, H. Miura, K. Sumioka, S. M. Zakeeruddin, M. Grätzel, *ACS Nano* **2008**, *2*, 1113.

[27] Y. H. Kwon, S. W. Woo, H. R. Jung, H. K. Yu, K. Kim, B. H. Oh, S. Ahn, S. Y. Lee, S. W. Song, J. Cho, H. C. Shin, J. Y. Kim, *Adv. Mater.* **2012**, *24*, 5192.
[28] S.-Y. Lee, K.-H. Choi, W.-S. Choi, Y. H. Kwon, H.-R. Jung, H.-C. Shin, J. Y. Kim, *Energy Environ. Sci.* **2013**, *6*, 2414.
[29] G. M. Zhou, F. Li, H.-M. Cheng, *Energy Environ. Sci.* **2014**, *7*, 1307.
[30] Y.-C. Lu, B. M. Gallant, D. G. Kwabi, J. R. Harding, R. R. Mitchell, M. S. Whittingham, Y. Shao-Horn, *Energy Environ. Sci.* **2013**, *6*, 750.
[31] Z. L. Wang, D. Xu, J. J. Xu, X. B. Zhang, *Chem. Soc. Rev.* **2014**, *43*, 7746.
[32] P. G. Bruce, S. A. Freunberger, L. J. Hardwick, J. M. Tarascon, *Nat. Mater.* **2012**, *11*, 19.
[33] J.-J. Xu, Z.-L. Wang, D. Xu, L.-L. Zhang, X.-B. Zhang, *Nat. Commun.* **2013**, *4*, 2438.
[34] J. Lu, L. Li, J.-B. Park, Y.-K. Sun, F. Wu, K. Amine, *Chem. Rev.* **2014**, *114*, 5611.
[35] F. J. Li, T. Zhang, H. S. Zhou, *Energy Environ. Sci.* **2013**, *6*, 1125.
[36] A. C. Luntz, B. D. McCloskey, *Chem. Rev.* **2014**, *114*, 11721.
[37] Y. Zhang, L. Wang, Z. Guo, Y. Xu, Y. Wang, H. Peng, *Angew. Chem., Int. Ed.* **2016**, *55*, 1.
[38] Q.-C. Liu, J.-J. Xu, D. Xu, X.-B. Zhang, *Nat. Commun.* **2015**, *6*, 7892.
[39] Q.-C. Liu, L. Li, J.-J. Xu, Z.-W Chang, D. Xu, Y.-B. Yin, X.-Y. Yang, T. Liu, Y.-S. Jiang, J.-M. Yan, X.-B. Zhang, *Adv. Mater.* **2015**, *27*, 8095.
[40] T. Liu, Q.-C. Liu, J.-J. Xu, X.-B. Zhang, *Small* **2016**, *12*, 3101.
[41] Z. Jian, P. Liu, F. Li, P. He, X. Guo, M. Chen, H. Zhou, *Angew. Chem., Int. Ed.* **2013**, *52*, 1.
[42] Z. Wu, D. Wang, W. Ren, J. Zhao, G. Zhou, F. Li, H. Cheng, *Adv. Funct. Mater.* **2010**, *20*, 3595.
[43] X. Guo, P. Liu, J. Han, Y. Ito, A. Hirata, T. Fujita, M. Chen, *Adv. Mater.* **2015**, *27*, 6137.
[44] J.-J. Xu, Z.-L. Wang, D. Xu, F.-Z. Meng, X.-B. Zhang, *Energy Environ. Sci.* **2014**, *7*, 2213.
[45] C. Xia, M. Waletzko, L. Chen, K. Peppler, P. J. Klar, J. Janek, *ACS Appl. Mater. Interfaces* **2014**, *6*, 12083.
[46] Z. Zhang, Z. Luo, B. Chen, C. Wei, J. Zhao, J. Chen, X. Zhang, Z. Lai, Z. Fan, C. Tan, M. Zhou, Q. Lu, B. Li, Y. Zong, C. Yan, G. Wang, Z. J. Xu, H. Zhang, *Adv. Mater.* **2016**, *28*, 8712.